Electronic Supplementary Material (ESI) for Journal of Materials Chemistry A.

Supplementary Information for

Novel high-performance Ga_2Te_3 anode for Li-ion batteries

*Young-Han Lee,[a,c] Yoon Hwa,[*b] and Cheol-Min Park*[*a,c]*

[a] School of Materials Science and Engineering, Kumoh National Institute of Technology, 61 Daehak-ro, Gumi, Gyeongbuk 39177, Republic of Korea

[b] School of Electrical, Computer, and Energy Engineering, Arizona State University, Tempe, AZ, 85281, USA

[c] Department of Energy Engineering Convergence, Kumoh National Institute of Technology, Gumi, Gyeongbuk 39177, Republic of Korea

[*]**Corresponding authors.**

Tel.: +82 (054) 478-7746. Fax: +82 (054) 478-7769. E-mail: cmpark@kumoh.ac.kr (C.-M. Park)

Tel.: +1 (602) 543-3490. E-mail: yoon.hwa@asu.edu (Y. Hwa)

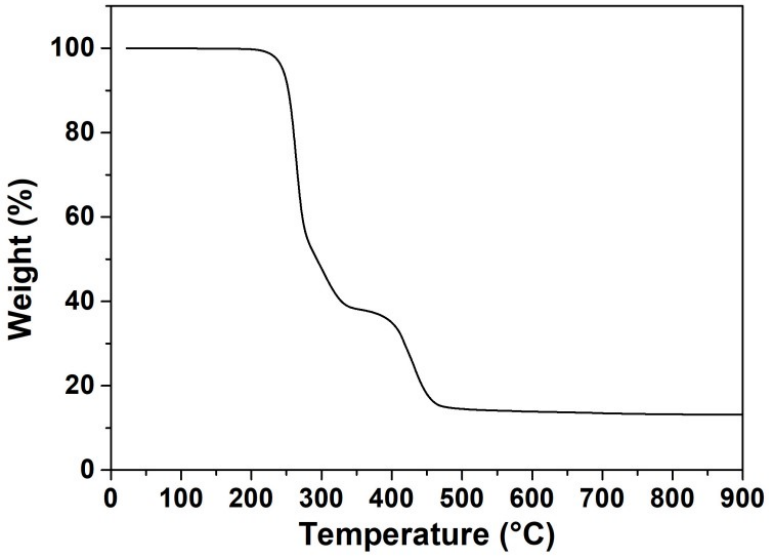

Figure S1. TGA data of pyrolyzed PVC, recorded between the ambient temperature and 900 °C.

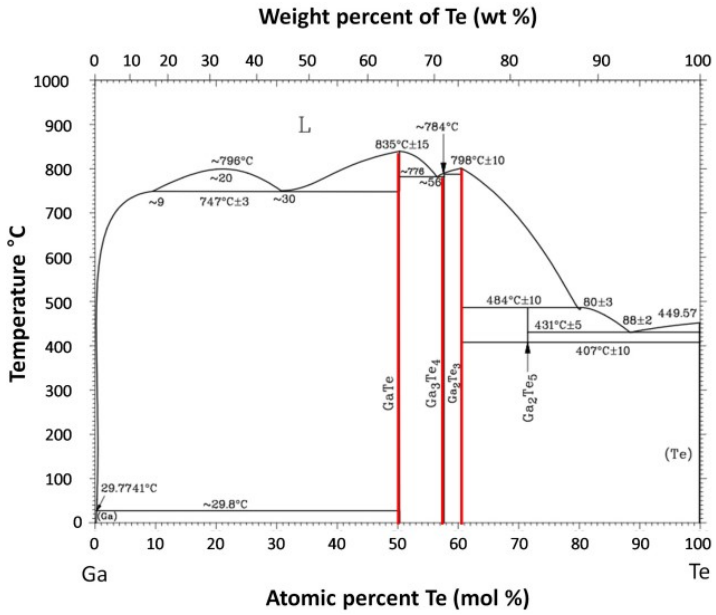

Figure S2. Binary phase diagram of Ga and Te, depicting thermodynamically stable GaTe, Ga_3Te_4, and Ga_2Te_3 phases at ambient temperature.

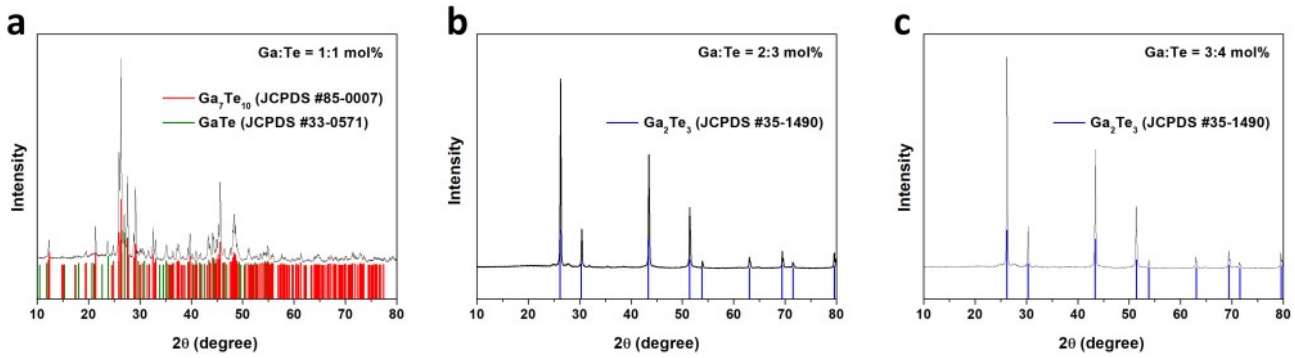

Figure S3. Synthesis of binary Ga-Te compounds and XRD results after heat-treatment of Ga and Te with different stoichiometric ratios (mol%): (a) 1:1; (b) 2:3; (c) 3:4.

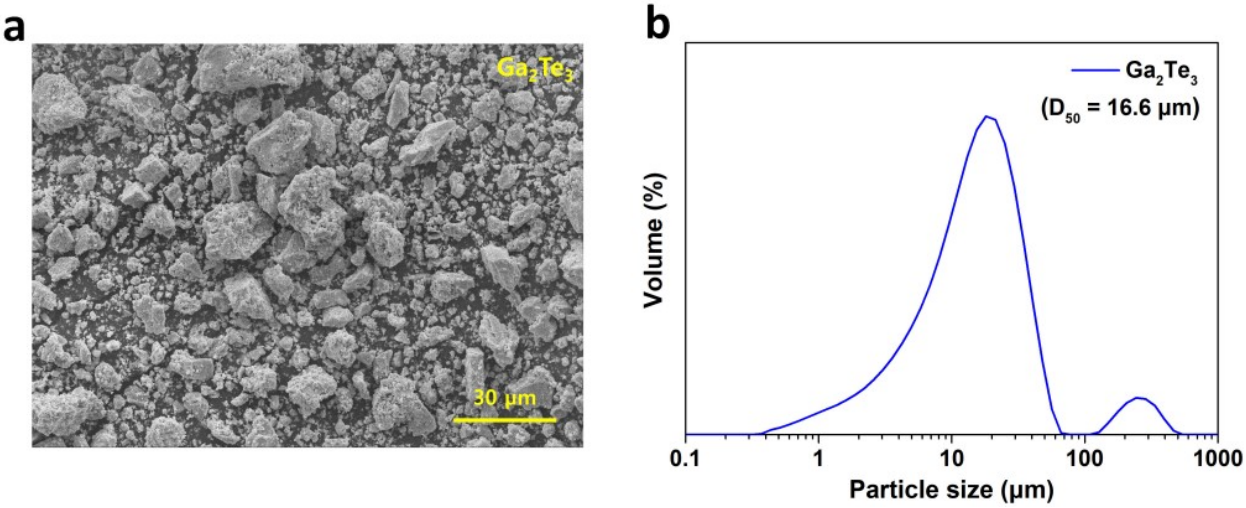

Figure S4. Characterization of synthesized Ga_2Te_3 powder: (a) SEM image; (b) result of particle size analysis.

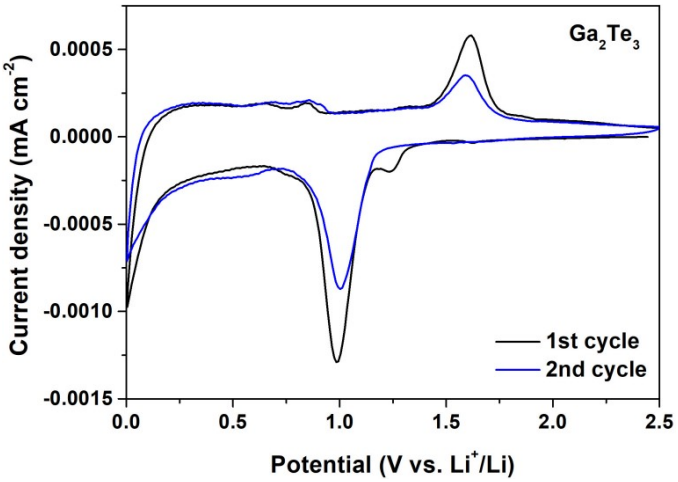

Figure S5. CV results for the first and second cycles of Ga_2Te_3 electrode for LIBs (voltage range: 0–2.5 V).

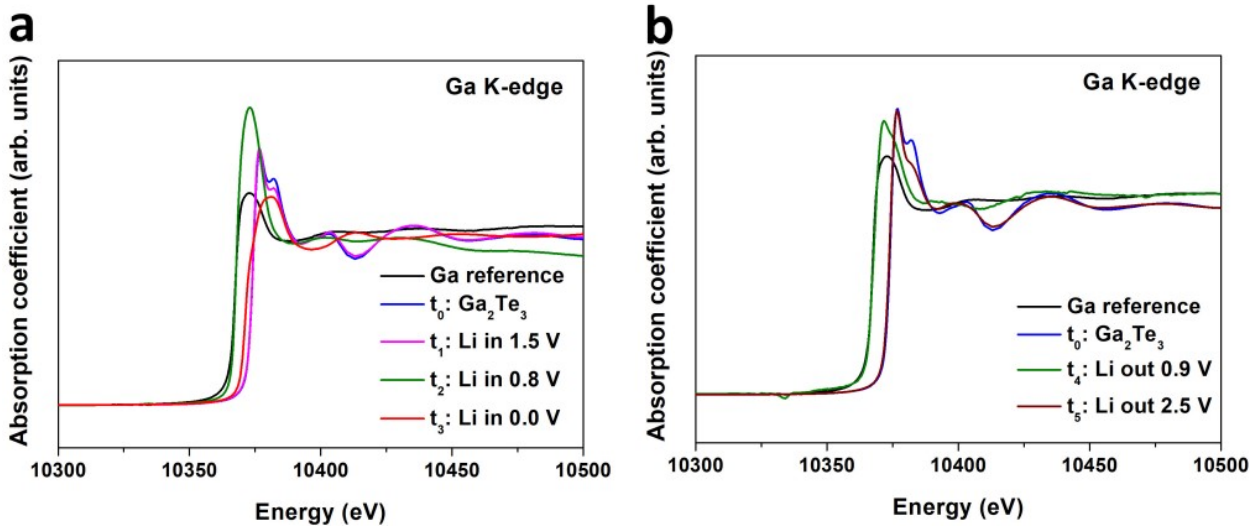

Figure S6. Reaction mechanism of Ga_2Te_3 anode with Li. Ga-K edge XANES spectra of Ga_2Te_3 anode during the first (a) lithiation and (b) delithiation processes.

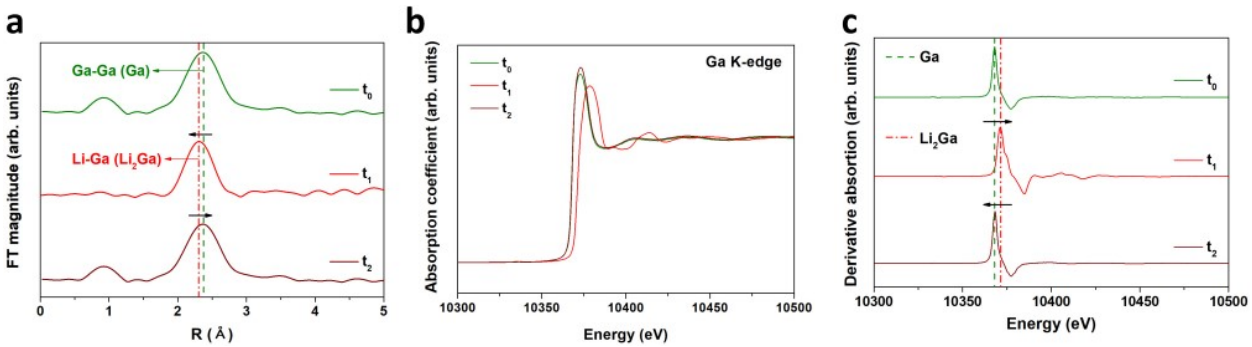

Figure S7. Reaction mechanism of Ga anode with Li. (a) *Ex situ* EXAFS results. (b) XANES spectra and (c) derivative XANES patterns of Ga anode collected at the selected potentials (t_0–t_2).

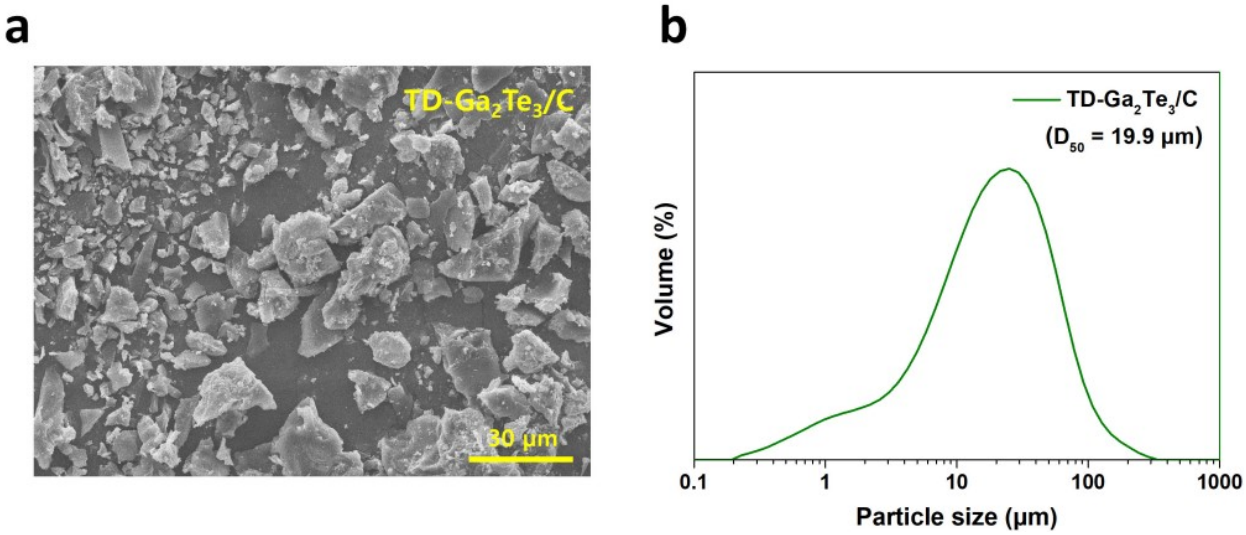

Figure S8. Characterization of synthesized TD-Ga_2Te_3/C powder. (a) SEM image. (b) Result of particle size analysis.

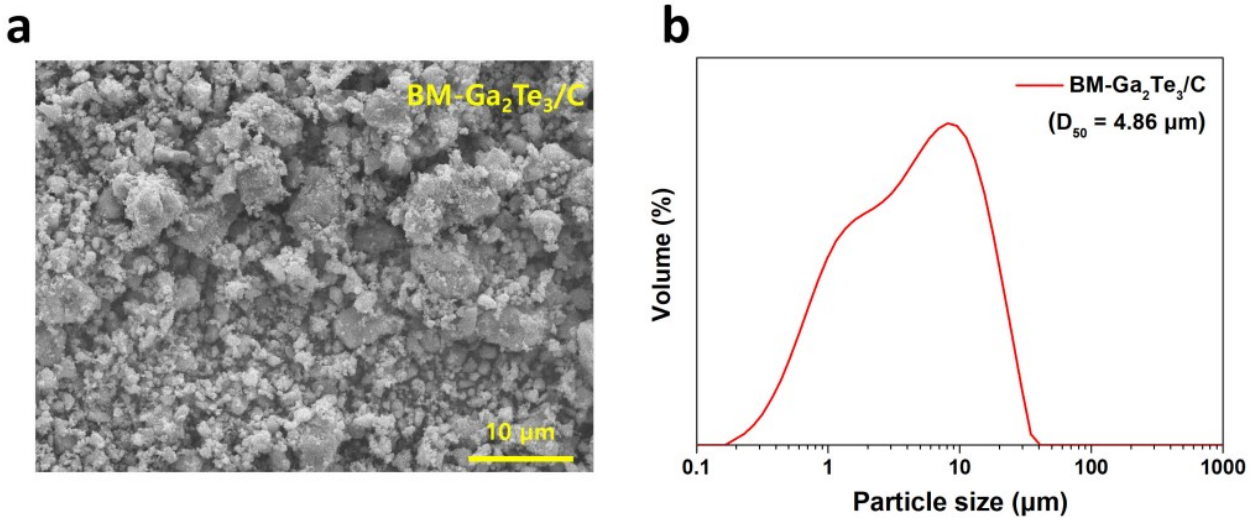

Figure S9. Characterization of synthesized BM-Ga_2Te_3/C powder. (a) SEM image. (b) Result of particle size analysis.

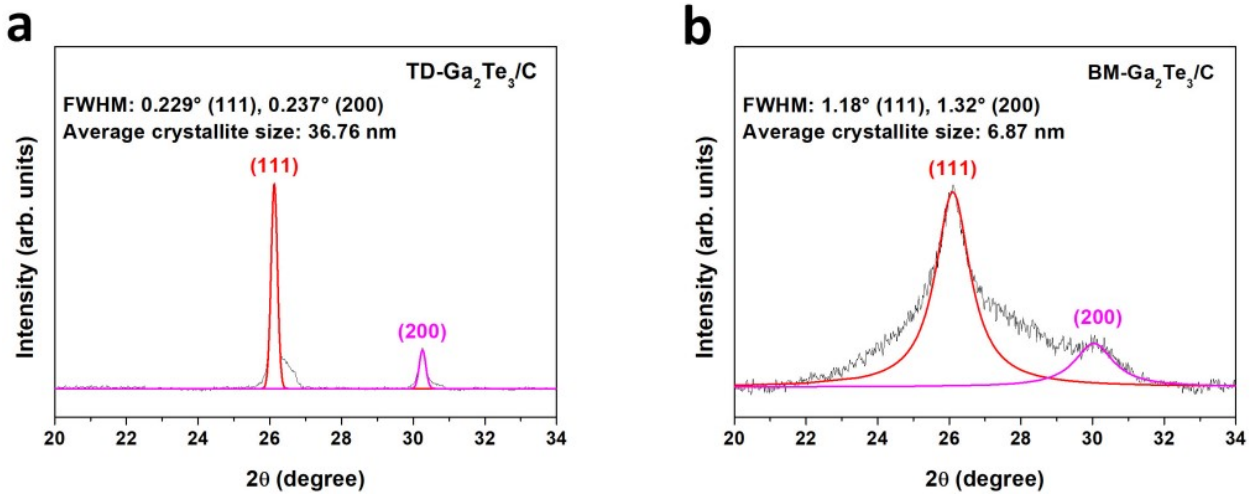

Figure S10. Crystallite size using XRD patterns of synthesized TD-Ga_2Te_3/C and BM-Ga_2Te_3/C composites. (a) Average crystallite size of Ga_2Te_3 in TD-Ga_2Te_3/C calculated using (111) and (200) planes of the XRD result. (b) Average crystallite size of Ga_2Te_3 in BM-Ga_2Te_3/C calculated using (111) and (200) planes of the XRD result.

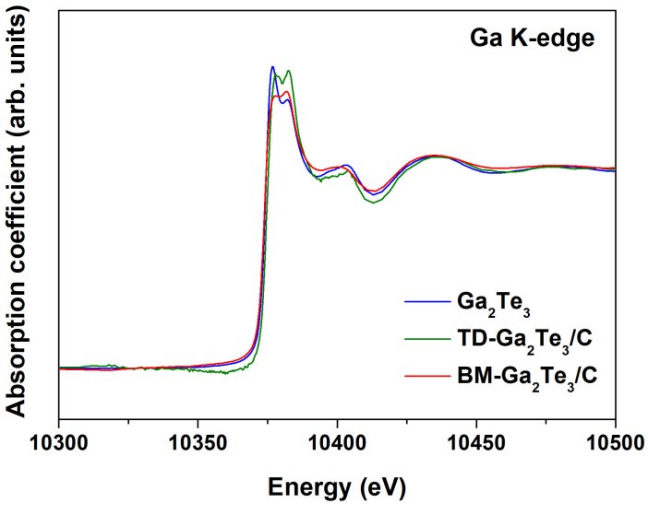

Figure S11. Synthesis of TD-Ga_2Te_3/C and BM-Ga_2Te_3/C composites. Ga-K edge XANES spectra for Ga_2Te_3, TD-Ga_2Te_3/C, and BM-Ga_2Te_3/C composites.

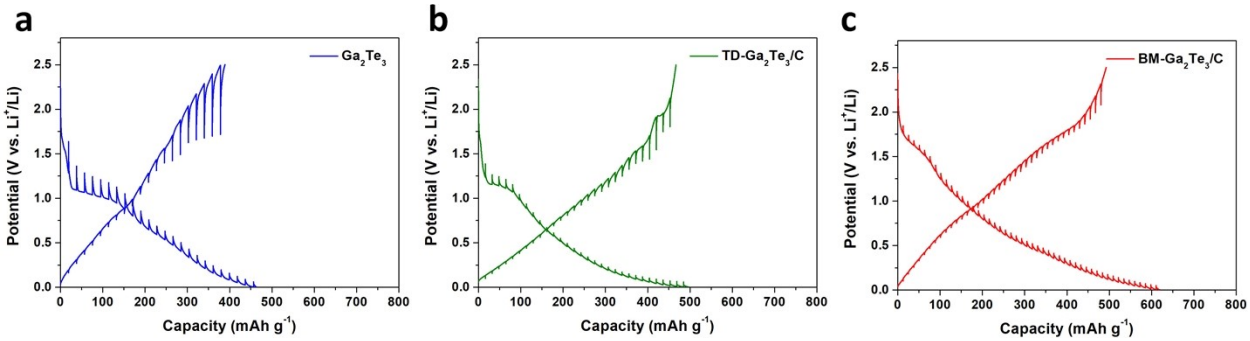

Figure S12. GITT plots of the Ga_2Te_3, TD-Ga_2Te_3/C, and BM-Ga_2Te_3/C composite anodes after 2 cycle at 100 mA g^{-1} (voltage range: 0–2.5 V). (a) GITT plot of the Ga_2Te_3 anode. (b) GITT plot of the TD-Ga_2Te_3/C anode. (c) GITT plot of the BM-Ga_2Te_3/C anode.

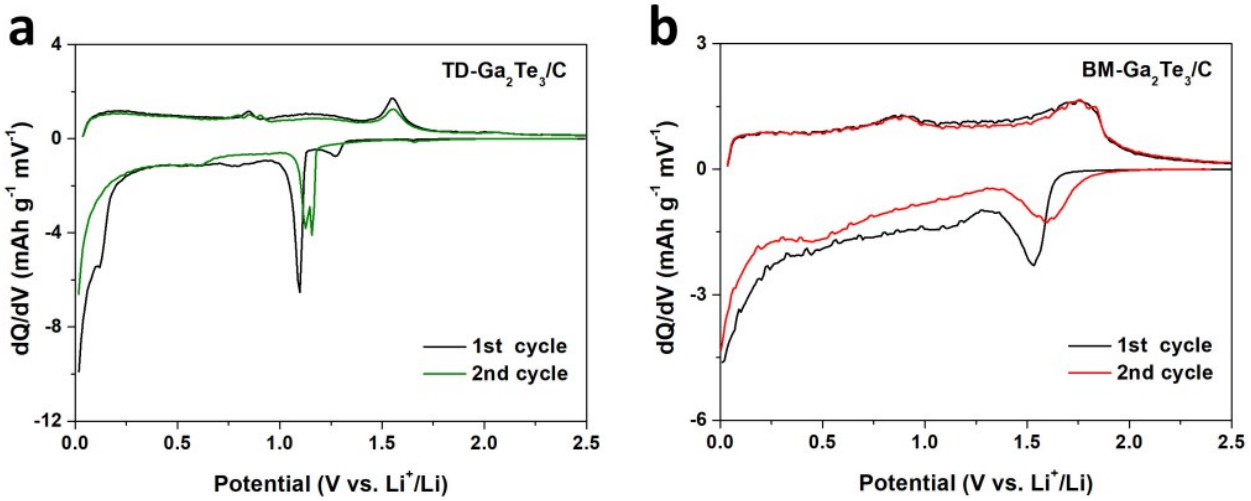

Figure S13. Differential capacity plots (DCPs) for TD-Ga_2Te_3/C and BM-Ga_2Te_3/C. (a) First and second DCPs of TD-Ga_2Te_3/C (voltage range: 0–2.5 V). (b) First and second DCPs of BM-Ga_2Te_3/C (voltage range: 0–2.5 V).

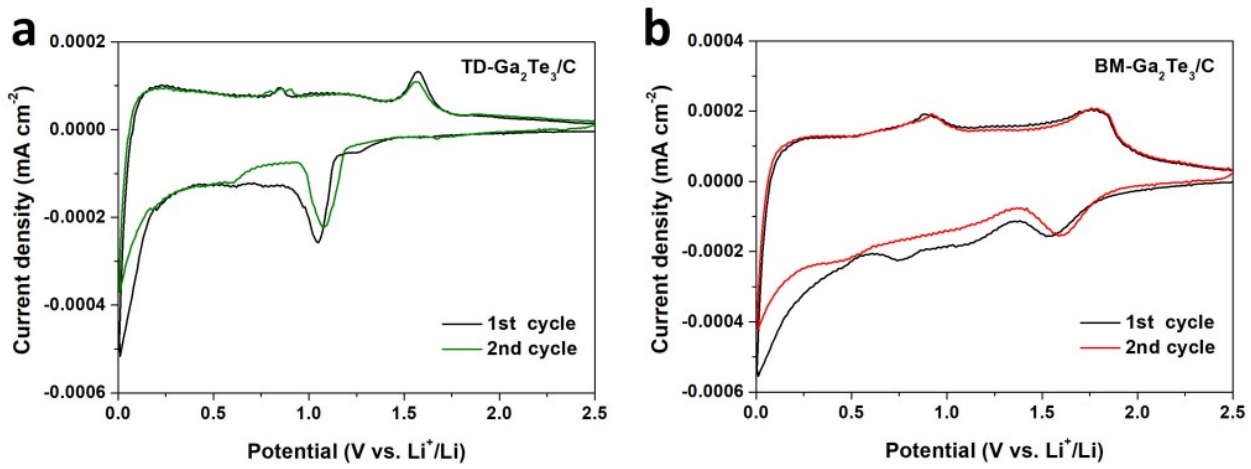

Figure S14. Cyclic voltammetry (CV) results for TD-Ga_2Te_3/C and BM-Ga_2Te_3/C. (a) First and second CV plots of TD-Ga_2Te_3/C (voltage range: 0–2.5 V). (b) First and second CV plots of BM-Ga_2Te_3/C (voltage range: 0–2.5 V).

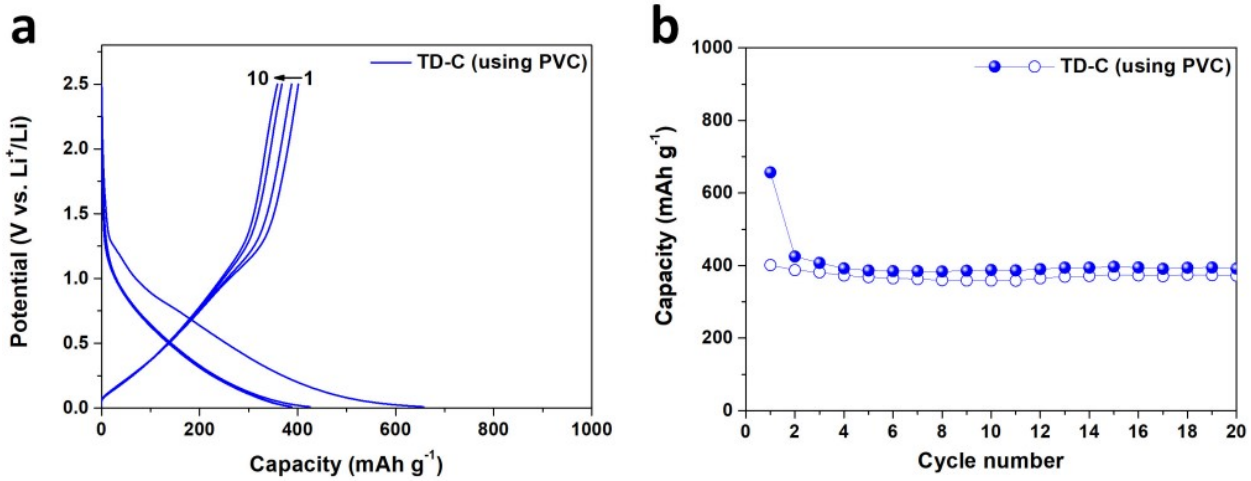

Figure S15. Electrochemical performance of thermally decomposed amorphous carbon produced by thermal decomposition (TD). (a) Voltage profile. (b) Cycling stability (current density: 100 mA g^{-1}).

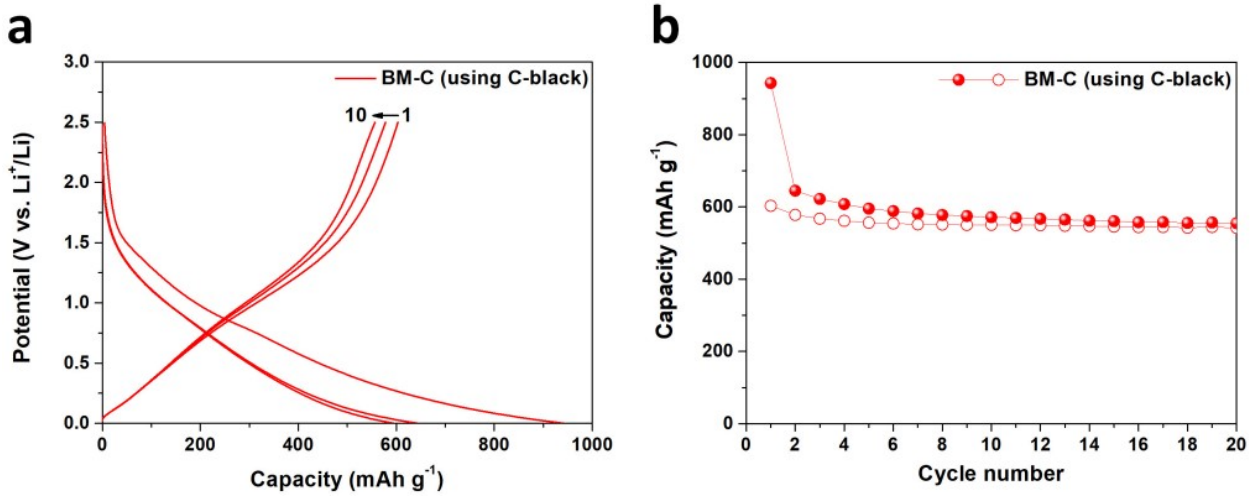

Figure S16. Electrochemical performance of ball milling (BM) treated amorphous carbon. (a) Voltage profile. (b) Cycling stability (current density: 100 mA g^{-1}).

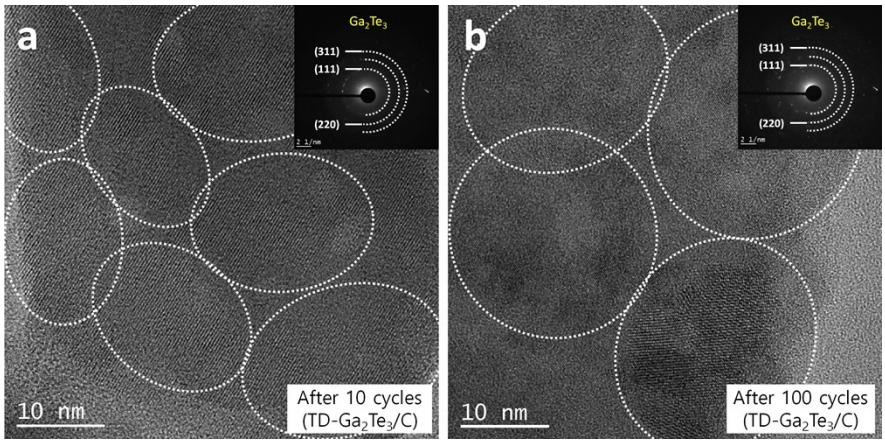

Figure S17. HRTEM images of TD-Ga_2Te_3/C composite anode after galvanostatic cycling. *Ex situ* HRTEM images of TD-Ga_2Te_3/C composite with SAEDs after (a) 10 and (b) 100 galvanostatic cycles.

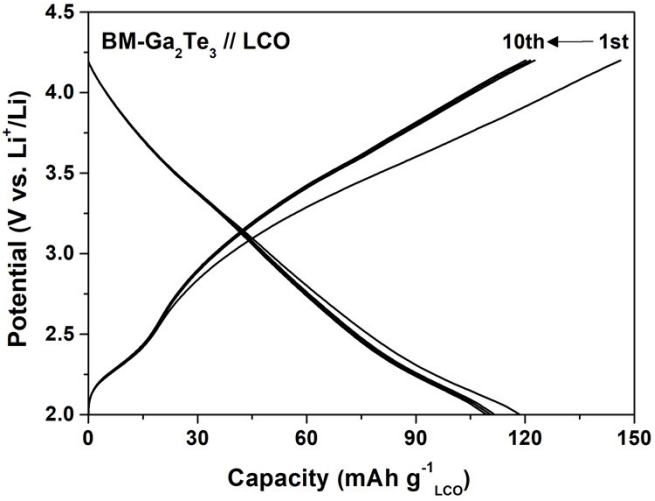

Figure S18. Electrochemical performance of full cell comprising of BM-Ga_2Te_3/C anode and LCO cathode. Voltage profile of the full cell with BM-Ga_2Te_3/C anode and LCO cathode within the potential range of 2.0–4.2 V at 0.1 C (=14 mA g^{-1}).

Supplementary Table 1: Comparison of electrochemical performances of various Ga-based anodes for LIBs.

Material	Cycling performance		Rate capability		Ref.
	Current density ($A\ g^{-1}$)	Reversible capacity after Xth cycles ($mAh\ g^{-1}$)	Current density ($A\ g^{-1}$)	Reversible capacity	
Ga-C NPs	0.1	400 (X=100)			14
Ga-In alloy	2.1	400 (X=500)	3.5	400	41
$CuGa_2$	0.2	550 (X=60)	2	500	42
GaN NWs/graphite	0.1	486 (X=400)	10	75	43
Ga_2O_3 NRs	0.1	300 (X=50)	1	243	44
Ga_2O_3/rGO	0.05	770 (X=40)	1	320	45
Ga_2O_3@C NPs	0.5	720 (X=200)	2	271	46
β-Ga_2O_3@G/C	0.2	517.9 (X=100)	0.5	376.7	47
α-Ga2O3@C@G	0.1	447.3 (X=50)	0.5	334.9	48
Ga_2S_3	0.1	400 (X=20)	1	550	49
SWCNT-GaS_x	0.12	575 (X=100)	0.6	514	50
GaS NS/SWCNT	1	300 (X=100)	2	530	51
GaSe NS/SWCNT	0.1	713 (X=5)	2	413	51
GaSe	0.1	760 (X=50)	1	600	52
Ga_2Se_3 thin film	0.07	569.9 (X=100)	0.7	340	53
BM-Ga_2Te_3/C (This work)	**0.1**	**574 (X=500)**	**0.6**	**528**	**-**